THE METHOD OF FUNDAMENTAL SOLUTIONS FOR WATER-WAVE DIFFRACTION BY THIN POROUS BREAKWATER

C. H. Tsai [*] **D. L. Young** [**]

Department of Civil Engineering & Hydrotech Research Institute
National Taiwan University
Taipei, Taiwan 10617, R.O.C.

ABSTRACT

The method of fundamental solutions (MFS) and domain decomposition method (DDM) are employed to solve the water-wave diffraction by a thin porous vertical breakwater of semi-infinite extent. Based on the linearized theory of water waves, the problem can be reduced to a boundary value problem with degenerate boundary. In contrast to other mesh dependent numerical method, the MFS is easier and more efficient to handle degenerate boundary value problems. Various incident wave angles and porous parameters are included to validate the power of the proposed numerical scheme. The present results demonstrate the MFS is sufficiently accurate and feasible to be used to predict water-wave diffraction by a thin permeable breakwater by comparing with literature.

Keywords : Method of fundamental solutions, Domain decomposition method, Porous breakwater, Water-wave diffraction, Degenerate boundary.

1. INTRODUCTION

MFS proposed by Kupradze and Aleksidze [1] is one of the most promising meshless numerical schemes, and is widely applied to many researches so far, including potential flow problems [2,3], biharmonic equations [4,5] and Poisson equations [6] *etc*. The essence of MFS is to decompose the solution of the given partial differential equations (PDEs) by means of superposition of the fundamental solution with proper intensities, called the point sources. Since these point sources are determined by collocating the known boundary data on a selected number of boundary points, the problem of interior mesh generation is completely eliminated, and this concept is similar to the boundary element method (BEM) to reduce one dimension. In contrast, MFS possesses all the merits of the BEM, but is free from singularity and the boundary element integration. Although MFS has been widely used to solve many kinds of boundary value problems, its application to problems with degenerate boundary is still very limited. Chen *et al.* [7] used the MFS and the domain decomposition method (DDM) to analyze the degenerate boundary problems for thin membranes in the presence of stringers at various orientations. Following the above scheme, Young *et al.* [8] solved the velocity potential equations to study flow nets generated in the presence of thin sheet piles. Furthermore, we extended the MFS in this paper to simulate this degenerate boundary problem which is difficult to be approached by other numerical schemes.

Detached porous breakwaters are usually parallel to the shore line to prevent coast line from erosion. When sea water impinges on a breakwater, the incident wave energy either gets reflected or dissipated, whereas the wave diffraction by the breakwater alters the wave direction and height. To analyze this problem, the linear potential wave theory is used to simplify the problem and makes it possible to be approached. Because the depth of porous thin breakwater is constant, the influence of depth can be neglected. Furthermore, when the wavelength of the incident waves is much greater than the thickness of the breakwaters, each segment of breakwater can be modeled as a thin vertical structure. Thus the problem can be reduced to a problem of two-dimensional wave diffraction by line segments. It is noted that exact solution for such problem only exists in simple geometry [9]. Yu [10] analyzed the diffraction of water waves by porous breakwaters via including the porosity effect to the porous boundary condition. McIver [11] employed an explicit solution method based on the Wiener-Hopf technique to obtain the solution of diffraction of an incident plane wave by a thin porous vertical breakwater of semi-infinite extent. McIver [12] further analyzed the solution for water-wave diffraction by breakwater which consists of four distinct elements, through deriving an integral equation for the potential of the diffracted field based on the Green's theorem. Chen *et al.* [13] adopted the dual boundary element method to study wave diffraction over a thin vertical and inclined breakwater with rigid boundary conditions.

[*] Graduate student [**] Professor, corresponding author

DOI : 10.1017/jmech.2011.16
Copyright © 2011 The Society of Theoretical and Applied Mechanics, R.O.C.
https://doi.org/10.1017/jmech.2011.16 Published online by Cambridge University Press

In this investigation, we combined the MFS with DDM [7,8,14,15] to simulate the solution of water-wave diffraction by solving the degenerate boundary value problems. By dividing the computational domain into two sub-domains, the singularity near the degenerate boundary can be eliminated, and thus the resulting matrices for both sub-domains can be formed by the MFS. By imposing the interface conditions and the boundary conditions into the resulting matrices, the global matrix system of linear algebraic equations can be solved by singular value decomposition (SVD) technique [16]. The governing equations are listed and explained in section 2. The description of the MFS and the concept of DDM are introduced in section 3. The comparisons of the results of applying the proposed method with benchmark solutions are presented in section 4, along with a further discussion of numerical issues. These will be seen to clearly demonstrate considerable improvements in the solvability of such type of difficult but interesting problem. Finally we summarize the findings in section 5.

2. GOVERNING EQAUTION

Assuming the fluid is ideal and the flow is irrotational, the flow field in the exterior of a breakwater can be completely described by a velocity potential $\mathrm{Re}\left\{\bar{\phi}_T(x, y, z)\, e^{(-i\omega t)}\right\}$ which satisfies the Laplace equation

$$\frac{\partial^2 \bar{\phi}_T}{\partial x^2}+\frac{\partial^2 \bar{\phi}_T}{\partial y^2}+\frac{\partial^2 \bar{\phi}_T}{\partial z^2}=0\ , \tag{1}$$

where ω is the frequency. A Cartesian coordinate system is employed, with *x*- and y-axes respectively lying in the transverse and longitudinal horizontal planes and the *z*-axis directing in the vertical direction. Figure 1 depicts the plane view of the semi-infinite porous medium where the breakwater occupies a region specified by $-\infty < x < 0$, $-b/2 < y < b/2$ and $-h < z < 0$, where *b* is the thickness of breakwater, and *h* is water depth. Because the wavelength of the incident wave is much greater than the thickness of the porous breakwater, the thin porous breakwater can be conducted as thin line segments. The boundary condition on the breakwater barrier can be expressed as

$$\begin{aligned}\frac{\partial \bar{\phi}_T}{\partial y}(x,\ 0^+,\ z) &= \frac{\partial \bar{\phi}_T}{\partial y}(x,\ 0^-,\ z)\\ &= \beta\left[\bar{\phi}_T(x,\ 0^+,\ z)-\bar{\phi}_T(x,\ 0^-,\ z)\right]\ ,\end{aligned} \tag{2}$$

for $-\infty < x < 0$, where the subscripts '+' and '$^-$' respectively indicate limits above and below a given boundary. The parameter β is defined as $\beta = -i\eta\ /\ [b(f - is)]$, where η is the porosity of the breakwater, *f* is a non-dimensional friction coefficient and *s* is a non-dimensional inertia coefficient. [In Yu's [10] notation $\beta = -ikG$, where *G* is the porous-wall-effect parameter].

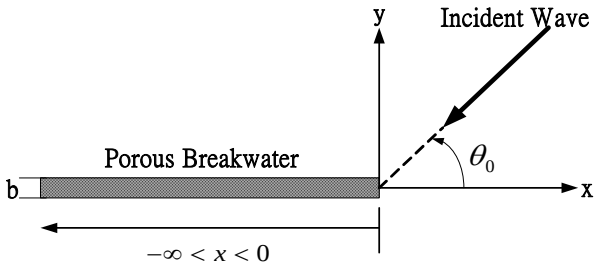


Fig. 1 Schematic of water-wave diffraction by thin porous breakwater

On the free surface, the velocity potential satisfies the linearized condition:

$$\frac{\partial \bar{\phi}_T}{\partial z}=\frac{\omega^2}{g}\bar{\phi}_T \quad \text{on} \quad z=0\ , \tag{3}$$

and on the bed, it satisfies the non-penetration condition:

$$\frac{\partial \bar{\phi}_T}{\partial z}=0 \quad \text{on} \quad z=-h\ , \tag{4}$$

where *g* is the acceleration induced by the gravity.

In the absence of transient modes in Eq. (2), for plane-wave incidence, the velocity potential throughout the fluid domain can be expressed as

$$\bar{\phi}_T(x,\ y,\ z)=\phi_T(x,\ y)\cosh k(z+h)\ , \tag{5}$$

where Eq. (5) satisfies the boundary conditions on both the free surface and the bed, and the depth dependence is neglected. By substituting Eq. (5) into Eq. (3), for a constant depth *h*, the wave number *k* satisfies the dispersion relation

$$\omega^2 = gk\tanh(kh)\ . \tag{6}$$

After substituting Eq. (5) into Eq. (1), we obtained a governing equation of ϕ_T which is a two-dimensional Helmholtz equation:

$$\frac{\partial^2 \phi_T}{\partial x^2}+\frac{\partial^2 \phi_T}{\partial y^2}+k^2\phi_T=0\ . \tag{7}$$

Theoretically, total potential ϕ_T in the breakwater problem is equal to the summation of the incident wave ϕ_I and the scattered wave ϕ_S. Hence the total potential is represented as

$$\phi_T=\phi_I+\phi_S\ , \tag{8}$$

where the incident velocity potential, ϕ_I, which is the solution of two-dimensional Helmholtz equation can be expressed as

$$\phi_I=\exp(-ikx\cos\theta_0-iky\sin\theta_0)\ , \tag{9}$$

and

$$\frac{\partial^2 \phi_I}{\partial x^2}+\frac{\partial^2 \phi_I}{\partial y^2}+k^2\phi_I=0\ , \tag{10}$$

https://doi.org/10.1017/jmech.2011.16 Published online by Cambridge University Press

where θ_0 represents the angle between the direction of the incident wave and x-axis.

After substituting Eq. (8) into Eq. (7), basing on Eq. (10), the scattered potential can be expressed as the solution of the Helmholtz equation

$$\frac{\partial^2 \phi_S}{\partial x^2} + \frac{\partial^2 \phi_S}{\partial y^2} + k^2 \phi_S = 0 \,. \tag{11}$$

After substituting Eq. (5) into Eq. (2), basing on Eqs. (8) and (9), the boundary conditions of scattered potential of Eq. (2) are simplified as follows:

$$\begin{aligned} &\frac{\partial \phi_S}{\partial y}(x,\ 0^+) = \frac{\partial \phi_S}{\partial y}(x,\ 0^-) \\ &= ik \sin\theta_0\, e^{-ikx\cos\theta_0} + \beta\left[\phi_S(x,\ 0^+) - \phi_S(x,\ 0^-)\right] \end{aligned} \tag{12}$$

for $-\infty < x < 0$.

In general, the radiation boundary condition is assumed as

$$\lim_{kr\to\infty} (kr)^{1/2} \left(\frac{\partial \phi_S}{\partial r} - ik\phi_S \right) = 0 \,, \tag{13}$$

where the radiation coordinate $r = \sqrt{x^2 + y^2}$.

3. NUMERICAL METHOD

The MFS is appropriate for the exterior domain problems, because it is free from the necessity of mesh generation, and theoretically satisfies the solutions at infinite domain. When the wave motion is considered as a single domain, it is necessary to derive a hypersingular equation for the thin breakwater. Generally, it is difficult for numerical method to tackle the hypersingular equation. Therefore, in the present numerical scheme, the concept of DDM technique is included to avoid the problem induced by the hypersingular equation. By decomposing the computational domain into two sub-domains along the thin porous breakwater, the boundary conditions of the breakwater appear explicitly. To obtain the solution of the total potential ϕ_T in Eq. (8), the scattered potential ϕ_S of Eq. (11) is necessary to be solved firstly. In the present case, the free space Green's function for the 2D Helmholtz equation formulated by the scattered potential (Eq. (11)) can be expressed as

$$-\nabla^2 G\left(|\vec{\mathbf{x}} - \vec{\boldsymbol{\xi}}| \right) - k^2 G\left(|\vec{\mathbf{x}} - \vec{\boldsymbol{\xi}}| \right) = \delta(\vec{\mathbf{x}} - \vec{\boldsymbol{\xi}}) \,, \tag{14}$$

where $G(r_j) = \frac{-i}{4} H_0^{(2)}(kr_j) = \frac{-i}{4}\left[J_0(kr_j) - iY_0(kr_j) \right]$ is the fundamental solution, $\delta(\vec{\mathbf{x}} - \vec{\boldsymbol{\xi}})$ is the Dirac delta function, $\vec{\mathbf{x}}$ is the position of the field point, $\vec{\boldsymbol{\xi}}$ is the position of the source point and $r_j = |\vec{\mathbf{x}} - \vec{\boldsymbol{\xi}}_j|$ is the distance between field and source points. In the fundamental solution, $H_0^{(2)}$ is called the second kind of Hankel function of order zero, J_0 is the Bessel function of the first kind of order zero, and Y_0 is the Bessel function of the second kind of order zero. Using the above formulations, the solution of MFS for the scattered potential ϕ_s can be obtained by

$$\phi_s(\mathbf{x}) = \sum_{j=1}^{N} \alpha_j^{\phi}\, G(r_j) \,, \tag{15}$$

and the normal derivative is given as the following formulation:

$$\frac{\partial \phi_s(x,\ y)}{\partial n} = \sum_{j=1}^{N} \alpha_j^{\phi} \frac{\partial G(r_j)}{\partial n} \,, \tag{16}$$

where

$$\frac{\partial G(r_j)}{\partial n} = \frac{\partial G(r_j)}{\partial r}\frac{\partial r}{\partial n} = -\left[\frac{\vec{r}\cdot\vec{n}}{4r} k \right]\left[Y_1(kr_j) + iJ_1(kr_j) \right] \,, \tag{17}$$

where J_1 is the Bessel function of the first kind of order one, Y_1 is the Bessel function of the second kind of order one, α_j^{ϕ} is the undetermined coefficient of source intensity and N is the number of source points. Figure 2(a) shows the schematic diagram of a general degenerate boundary problem in water-wave diffraction by thin porous breakwater. In order to solve the solution of MFS for a general boundary value problem, N boundary field points are collocated to solve the Eq. (15). To a degenerate boundary value problem, the DDM [7,8,14,15] can be used to eliminate the singularity generated along the thin boundary. To investigate this degenerate problem, we decomposed the computational domain into two computational regions Ω_1 and Ω_2 along the section A-A, which is fictitious and used to divide the breakwater into two regions.

The schematic description for the DDM technique is illustrated in Fig. 2(b), as shown in the figure, ϕ_b^1 、 ϕ_f^1 and t_f^1 belong to Ω_1, similarly, ϕ_b^2 、 ϕ_f^2 and t_f^2 belong to Ω_2. On the sub-domain, Ω_1, ϕ_b^1 represents the value of the Dirichlet condition at boundary points 1 ~ 5, and ϕ_f^1 and t_f^1 respectively indicate the value of Dirichlet and Neumann condition at fictitious points 6 ~ 9. By similarity, ϕ_b^2 represents the value of Dirichlet condition at boundary points 1' ~ 5', and ϕ_f^2 and t_f^2 respectively indicate the value of Dirichlet and Neumann condition at fictitious points 6' ~ 9' on the sub-domain, Ω_2. At the interfacial boundary between these two sub-domains, the values of Dirichlet condition, ϕ, and Neumann condition, t, on Ω_1 are equal to the values on Ω_2, *i.e.* $\phi_b^1 = \phi_b^2$, $\phi_f^1 = \phi_f^2$ and $t_f^1 = t_f^2$. Based on the above relationships, the sub-domains Ω_1 and Ω_2 can be connected and considered as a single computational domain. Based on the relation between Eqs. (15) and (17), the approximate solution of MFS for both individual sub-domain can be expressed in matrix

https://doi.org/10.1017/jmech.2011.16 Published online by Cambridge University Press

form:

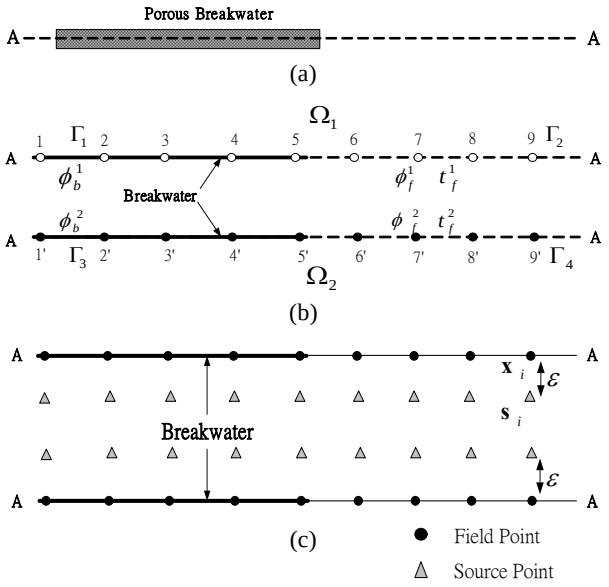


Fig. 2 The schematic diagram of (a) section A-A (b) domain decomposition method (c) field points and source points

$$[A_{ij}^{\Omega_1}]\{\alpha_j^{\Omega_1}\} = \begin{bmatrix} A_{ij}|_{\Gamma_1} \\ A_{ij}|_{\Gamma_2} \end{bmatrix} \{\alpha_j^{\Omega_1}\} = \begin{Bmatrix} \phi_b^1 \\ \phi_f^1 \\ t_f^1 \end{Bmatrix}, \tag{18}$$

$$[A_{ij}^{\Omega_2}]\{\alpha_j^{\Omega_2}\} = \begin{bmatrix} A_{ij}|_{\Gamma_3} \\ A_{ij}|_{\Gamma_4} \end{bmatrix} \{\alpha_j^{\Omega_2}\} = \begin{Bmatrix} \phi_b^2 \\ \phi_f^2 \\ t_f^2 \end{Bmatrix}, \tag{19}$$

where the coefficient matrices $[A_{ij}^{\Omega_1}]$ and $[A_{ij}^{\Omega_2}]$ contain the summation of the radial basis functions for the Helmholtz equation for the sub-domains Ω_1 and Ω_2, respectively, Γ_1 and Γ_2 are the physical and fictitious boundaries on sub-domains Ω_1, Γ_3 and Γ_4 are the physical and fictitious boundaries on sub-domains Ω_2 and $\{\alpha_j^{\Omega_1}\}$ and $\{\alpha_j^{\Omega_2}\}$ are the intensities of point sources of the sub-domains Ω_1 and Ω_2, respectively. The above equations have to be solved by considering the following connection conditions:

$$\{\phi_f^1\} = \{\phi_f^2\} \tag{20}$$

and

$$\{t_f^1\} = \{t_f^2\} \tag{21}$$

Using the DDM and combining Eqs. (16) ~ (21), the final equations for the entire computational domain can be obtained in matrix form as:

$$\begin{bmatrix} A_{ij}^{\Omega_1}|_{\Gamma_1} & 0 \\ 0 & A_{ij}^{\Omega_2}|_{\Gamma_3} \\ A_{ij}^{\Omega_1}|_{\Gamma_2} & -A_{ij}^{\Omega_2}|_{\Gamma_4} \end{bmatrix} \begin{bmatrix} \alpha_j^{\Omega_1} \\ \alpha_j^{\Omega_2} \end{bmatrix} = \begin{bmatrix} \phi_b^1 \\ \phi_b^2 \\ 0 \end{bmatrix} \tag{22}$$

Then, we uniformly distribute the boundary field points $\mathbf{x}_i$ to both the sub-domains and locate the source point $\mathbf{s}_i$ by calculating the formula $\mathbf{s}_i = \mathbf{x}_i \pm \varepsilon$, where ε is a parameter. Once the parameter, ε, is determined, the distributions of the source points can be obtained, as depicted in Fig. 2(c). After determining the positions of boundary field points and source points, the resulting matrix of linear equations is established by Eqs. (15) and (16). Through the SVD technique [16], the resulting ill-conditioned matrix system is solved, and then the values of α_j to the solutions of the scattered potential ϕ_s are obtained. Therefore, the total potential for the water-wave diffraction can be acquired from Eq. (8).

4. RESULTS AND DISCUSSIONS

The proposed numerical scheme based on the MFS and DDM technique is validated by considering some test problems of which results are available in the literature, including the exact solution presented by Penney and Price [17] and the results by boundary layer method proposed by Yu [10]. Various incident wave angles θ_0 and porous parameters β/k are included to test the feasibility of this numerical scheme. With a normal incident wave $\theta_0 = \pi/2$ and porous parameter $\beta/k = 0$, we used the number of collocation points $N = 80$ and $\varepsilon = 6.5$ to simulate the problem. Figures 3(a) and 3(b) show the comparisons of wave height at $y = \pm 4L$ between the results of the MFS and others [10,17]. As shown in Figs. 3(a) and 3(b), the results obtained by MFS closely agree with the results from [10,17]. Furthermore, in Fig. 4, the distributions of wave height near the tip of the impermeable breakwater ($\beta/k = 0$) are displayed in Fig. 4(a), and that for the permeable breakwater ($\beta/k = 0.1$) are plotted in Fig. 4(b). When the value of permeability increases up to 0.1, the behavior of wave along the permeable breakwater is obviously different from that along the impermeable breakwater. To clearly show the difference between these porous parameter, $\beta/k = 0.1$ and $\beta/k = 0$, Figs. 5(a) and 5(b) show the comparisons of the value $|\phi_T|$ at $y = \pm 4L$. As shown in Fig 5(a), the behavior of the water wave for permeable breakwater is more rugged than that for impermeable breakwater. Comparing the result at $y = 4L$ with that at $y = -4L$, the difference induced by permeability is clearly revealed. In addition, the performances of the results satisfy the physical phenomenon that permeability changes the behavior for water-wave diffraction behind the breakwater, as expected. The numerical results demonstrate that MFS is accurate and sufficient to be used to predict the water-wave diffraction by a thin permeable breakwater.

To further test the feasibility of the MFS to predict the water-wave diffraction, different porous parameters $\beta/k = 0$ and $0.25(1 - i)$, and incident angles $\theta_0 = \pi/4$ and $\theta_0 = 3\pi/4$ are considered in the following numerical experiments. In terms of the collocation points, $N = 80$ and $\varepsilon = 6.5$ are chosen to simulate this problem. Figure 6 shows the distributions of wave height around the tip of the breakwater with $\theta_0 = \pi/4$. The results for $\beta/k = 0$ and $0.25(1 - i)$ are plotted in Figs. 6(a) and 6(b),

https://doi.org/10.1017/jmech.2011.16 Published online by Cambridge University Press

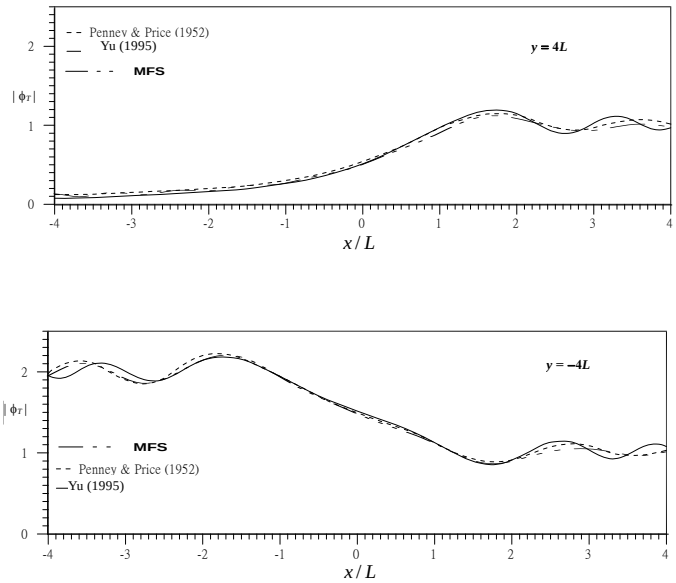


Fig. 3 The results for $\theta_0 = \pi/2$, $\beta/k = 0$ are compared with exact solutions [Penney and Price [17]] and results [Yu [10]]: (a) at $y = +4L$; (b) at $y = -4L$ ($N = 80$, $\varepsilon = 6.5$)

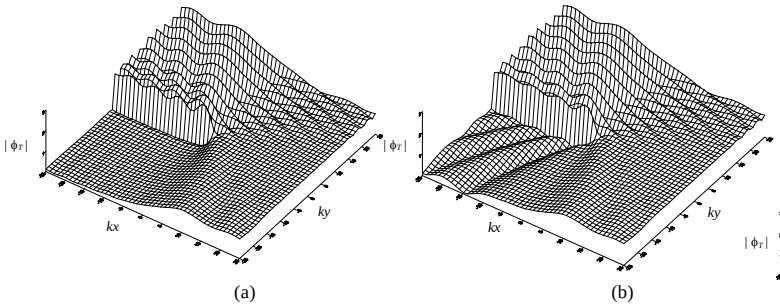


Fig. 4 Distribution of modulus value of total potential ϕ_T around the tip: (a) $\theta_0 = \pi/2$, $\beta/k = 0$ (b) $\theta_0 = \pi/2$, $\beta/k = 0.1$ ($N = 80$, $\varepsilon = 6.5$)

respectively. Comparing the results from Fig. 6 with the results from Fig. 4, it is obvious that the behavior of wave behind the breakwater becomes more rugged, and the reason is that the incident angle has been changed from $\theta_0 = \pi/2$ to $\theta_0 = \pi/4$. In addition, there exists a uniform increase to the wave amplitude behind the breakwater, and it is induced by the transition of wave energy. The comparisons of the modulus for total potential ϕ_T at $y = \pm 4L$ with different porous parameter are shown in Fig. 7. In contrast to the results from Fig. 5, the distributions of wave height are smoother and the value of $|\phi_T|$ are obviously less. The reason is that the energy of reflection decreases when the incident angle decreases from $\theta_0 = \pi/2$ to $\theta_0 = \pi/4$, and this behavior matches the real situation in physics, as expected.

Figure 8 shows the distributions of wave height near the tip of the breakwater when the value of incidence angle is further increased to $\theta_0 = 3\pi/4$, and two porous parameters, $\beta/k = 0$ and $0.25(1-i)$, are considered. $N = 120$ and $\varepsilon = 15$ are adopted to approach the solution of this problem. In contrast to the results of Figs. 4 and 6, more folds are generated behind the breakwater, and the results indicate the diffraction dominates the behavior

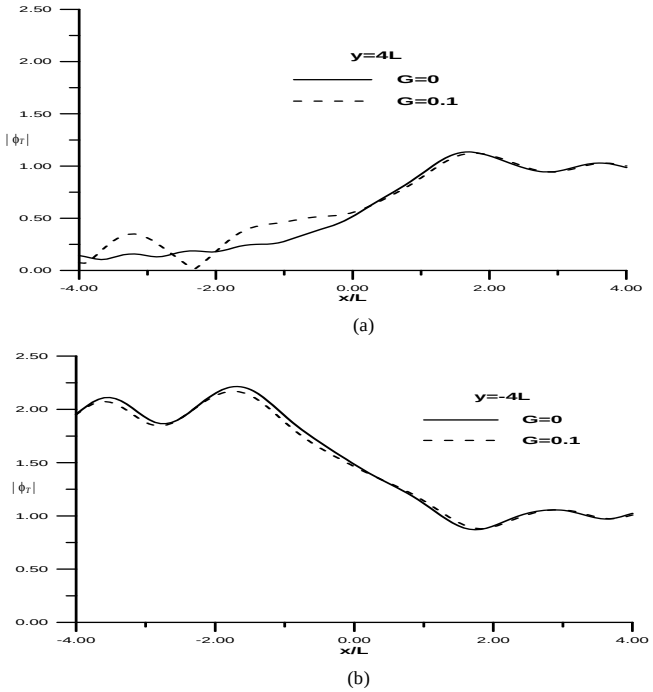


Fig. 5 The modulus value of total potential ϕ_T to the problem with $\theta_0 = \pi/2$ for $\beta/k = 0$ and $\beta/k = 0.1$: (a) at $y = 4L$; (b) at $y = -4L$ ($N = 80$, $\varepsilon = 6.5$)

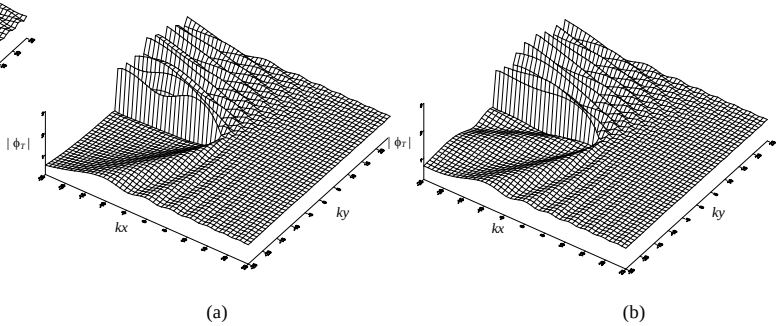
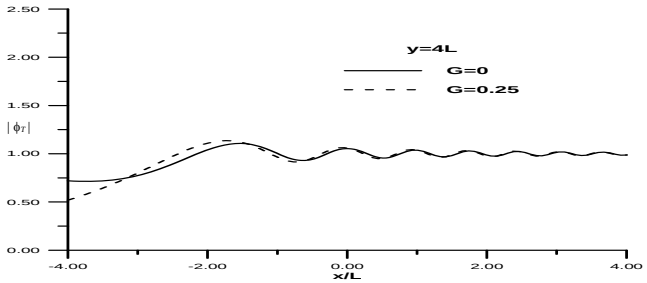


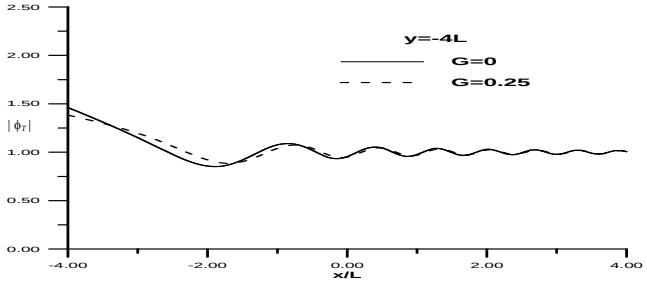
Fig. 6 Distribution of modulus value for total potential ϕ_T around the tip: (a) $\theta_0 = \pi/4$, $\beta/k = 0$ (b) $\theta_0 = \pi/4$, $\beta/k = 0.25(1-i)$ ($N = 80$, $\varepsilon = 6.5$)

of the wave under this incident angle. Figure 9 displays the comparisons for the values of $|\phi_T|$ at $y = \pm 4L$ between impermeable breakwater and permeable one. As shown in Fig. 9(a), the value of $|\phi_T|$ at $y = 4L$ increases more when the porous parameter increases from $\beta/k = 0$ to $\beta/k = 0.25(1-i)$. On the other hand, in terms of the results in Fig. 9(b), the value of $|\phi_T|$ at $y = -4L$ increases more when the porous parameter decreases from $\beta/k = 0.25(1-i)$ to $\beta/k = 0$. These results reveal that degree of permeability determines the generation of diffraction behind the breakwater. In other words, the behavior of the wave behind the breakwater is dominated by the diffraction of water wave. Conclusively, the present numerical scheme which combines the MFS with DDM can not only be used to accurately obtain the solution of water-wave diffraction behind a thin porous breakwater, but also can be employed to predict the real wave motion in physics.

https://doi.org/10.1017/jmech.2011.16 Published online by Cambridge University Press

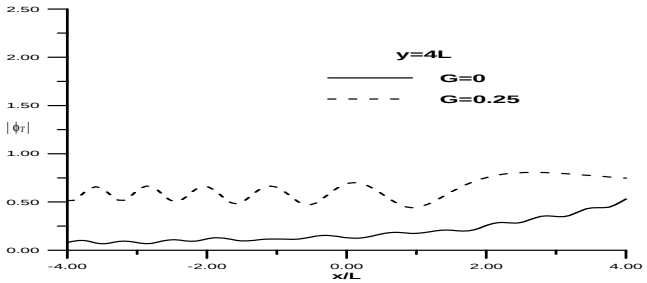


(a)

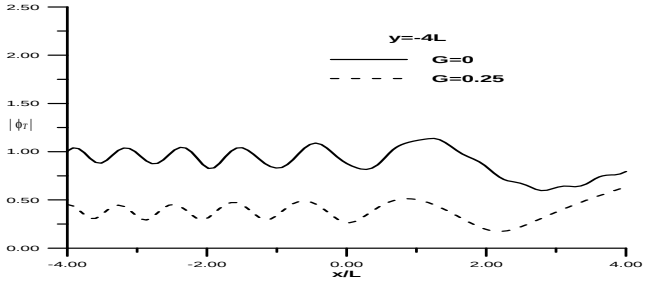


(b)

Fig. 7 The modulus value of total potential ϕ_T to the problem with $\theta_0 = \pi/4$ for $\beta/k = 0$ and $\beta/k = 0.25(1 - i)$: (a) at $y = +4L$; (b) at $y = -4L$ ($N = 80$, $\varepsilon = 6.5$)

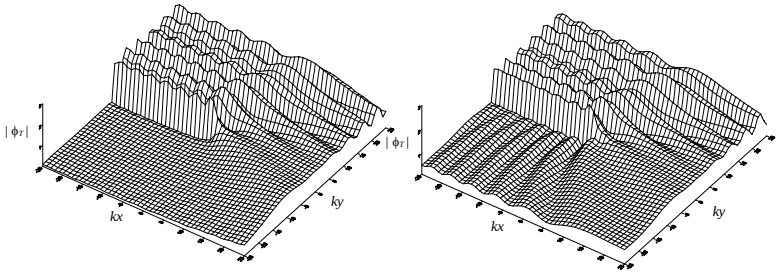


(a)



(b)

Fig. 9 The modulus value for total potential ϕ_T to the problem with $\theta_0 = 3\pi/4$ for $\beta/k = 0$ and $\beta/k = 0.25(1 - i)$: (a) at $y = +4L$; (b) at $y = -4L$ ($N = 120$, $\varepsilon = 15$)



(a) (b)

Fig. 8 Distribution of modulus value for total potential ϕ_T around the tip: (a) $\theta_0 = 3\pi/4$, $\beta/k = 0$ (b) $\theta_0 = 3\pi/4$, $\beta/k = 0.25(1 - i)$ ($N = 120$, $\varepsilon = 15$)

5. CONCLUSIONS

The method of fundamental solutions is successfully combined with domain decomposition method to simulate the water-wave diffraction by thin porous breakwaters. Through the assumption of linearized theory, the problem can be considered as a degenerate boundary value problem, and then the solution of the water-wave diffraction can be approached numerically. Comparing the solution of MFS with the benchmark solution presented in the literature, the numerical results demonstrate the proposed scheme is sufficient to be employed to tackle such degenerate boundary problems with various incident angles and porous parameters. In the future, the present work will be used to obtain the water-wave diffraction by a special medium finite length breakwater or by a gap in an infinite breakwater. Moreover, the present scheme will be also extended to solve other types of partial differential equations with degenerate boundary.

ACKNOWLEDGEMENTS

This research was partially supported by the National Science Council in Taiwan through the Grant NSC 96-2622-E-002-017-CC3 and NSC 96-2221-E-002-116-. It is greatly appreciated.

REFERENCES

1. Kupradze, V. D. and Aleksidze, M. A., "The Method of Functional Equations for the Approximate Solution of Certain Boundary Value Problem," *USSR Computational Mathematics and Mathematical Physics*, **4**, pp. 82–126 (1964).
2. Johnston, R. L. and Fairweather, G., "The Method of Fundamental Solutions for Problems in Potential Flow," *Applied Mathematical Modelling*, **8**, pp. 265–270 (1984).
3. Karageorghis, A. and Fairweather, G., "The Method of Fundamental Solutions for the Solution of Nonlinear Plane Potential Problems," *IMA Journal of Numerical Analysis*, **9**, pp. 231–242 (1989).
4. Karageorghis, A. and Fairweather, G., "The Almansi Method of Fundamental Solutions for Solving Biharmonic Problems," *International Journal for Numerical Methods in Engineering*, **26**, pp. 1665–1682 (1988).
5. Karageorghis, A. and Fairweather, G., "The Simple Layer Potential Method for Fundamental Solutions for Certain Biharmonic Problems," *International Journal for Numerical Methods Fluids*, **9**, pp. 1221–1234 (1989).

https://doi.org/10.1017/jmech.2011.16 Published online by Cambridge University Press

6. Golberg, M. A., "The Method of Fundamental Solutions for Poisson's Equation," *Engineering Analysis with Boundary Elements*, **16**, pp. 205–213 (1995).
7. Chen, C. W., Fan, C. M., Young, D. L., Murugesan, K. and Tsai, C. C., "Eigenanalysis for Membranes with Stringers Using the Methods of Fundamental Solutions and Domain Decomposition," *CMES-Computer Modeling in Engineering and Sciences*, **8**, pp. 29–44 (2005).
8. Young, D. L., Fan, C. M., Tsai, C. C. and Chen, C. W., "The Method of Fundamental Solutions and Domain Decomposition Method for Degenerate Seepage Flow Net Problems," *Journal of the Chinese Institute of Chemical Engineers*, **29**, pp. 63–73 (2006).
9. Havelock, T. H., "The Pressure of Water Waves upon a Fixed Obstacle," *Proceedings of the Royal Society of London. Series A, England*, **175**, pp. 409–421 (1940).
10. Yu, X., "Diffraction of Water Waves by Porous Breakwaters," *Journal of Waterway, Port, Coastal, and Ocean Engineering*, **121**, pp. 275–282 (1995).
11. McIver, P., "Water-wave Diffraction by Thin Porous Breakwater," *Journal of Waterway, Port, Coastal, and Ocean Engineering*, **125**, pp. 66–70 (1999).
12. McIver, P., "Diffraction of Water Waves by a Segmented Permeable Breakwater," *Journal of Waterway, Port, Coastal, and Ocean Engineering*, **131**, pp. 69–76 (2005).
13. Chen, K. H., Chen, J. T., Lin, S. Y. and Lee, Y. T., "Dual Boundary Element Analysis of Normal Incident Wave Passing a Thin Submerged Breakwater with Rigid, Absorbing, and Permeable Boundaries," *Journal of Waterway, Port, Coastal, and Ocean Engineering*, **130**, pp. 179–190 (2004).
14. Chan, T. F., Glowinski, R., Periaux, J. and Widlund, O. B., Domain Decomposition Methods for Partial Differential Equations, SIAM, Philadelphia (1989).
15. Chan, T.F., Glowinski, R., Periaux, J. and Widlund, O.B., Domain Decomposition Methods, SIAM, Philadelphia (1990).
16. Ramachandran, P. A., "Method of Fundamental Solutions: Singular Value Decomposition Analysis," *Communications in Numerical Methods in Engineering*, **18**, pp. 789–801 (2002).
17. Penney, W. G. and Price, A. T., "The Diffraction Theory of Sea Waves and the Shelter Afforded by Breakwaters," *Philosophical Transactions of the Royal Society of London, Series A, England*, **244**, pp. 236–253 (1952).

(Manuscript received July 20, 2010,
accepted for publication September 20, 2010.)

https://doi.org/10.1017/jmech.2011.16 Published online by Cambridge University Press